on electromagnetic fields induced inside finite biological bodies," *IEEE Trans. Microwave Theory Tech.*, vol. MTT-24, pp. 433–440, July 1976.
[11] K.-M. Chen and B. S. Guru, "Internal EM field and absorbed power density inside human torsos induced by 1 to 500 MHz EM waves," Division of Engineering Research, Michigan State University, East Lansing, MI, NSF Tech. Rep., 1976.
[12] O. P. Gandhi, "Condition of strongest electromagnetic power deposition in man and animals," *IEEE Trans. Microwave Theory Tech.*, vol. MTT-23, pp. 1021–1029, Dec. 1975.

Modal Characteristics of Crossed Rectangular Waveguides

FENG-LING CHENG LIN

Abstract—**The modal solution for the crossed rectangular waveguide is presented. Cutoff frequencies and modal fields are determined by formulating an integral eigenvalue equation which can be solved by application of the Ritz–Galerkin method. Field equations are given for both TE and TM modes. The calculated cutoff frequencies of several lower order modes agree very well with the available experimental results in the literature.**

I. Introduction

In PHASED ARRAY antenna systems, open-ended waveguides are commonly used as the radiating elements. In order to provide dual-polarization capability, circular or square waveguides are used because they can support two orthogonal modes [1]. In addition, a wide bandwidth is required for the propagation of the dominant mode.

It has been known for years that ridged waveguides have been useful in microwave systems due to their wide bandwidth properties. For double-ridged waveguide, the TE_{10}-TE_{20} modal bandwidth is increased with the ridge loading. However, a system capable of operating in two polarizations is desirable in practical applications. Thus the waveguide with a 90° rotational symmetry is adopted. Chen *et al.* [2] have performed detailed modal analysis on quadruple-ridged circular and square waveguides by means of Silvester's finite element program [3]. It was shown that for square waveguides, quadruple-ridged loading always decreases the TE_{10}–TE_{11} bandwidth, whereas for circular waveguides, a finite amount of additional separation between TE_{11} and TM_{01} modes can be achieved when the ridge dimensions are chosen properly.

The crossed rectangular waveguide possesses 90° rotational symmetry, thus providing dual-polarization properties. It can also be viewed as ridged waveguide with square ridges loading its corners. It is of physical interest to investigate the modal characteristics and to determine the cutoff frequencies and the transverse field patterns.

With the complete knowledge of the waveguide's eigenvalue spectrum, one can solve many problems currently encountered. One such problem for instance, is the radiation of crossed rectangular waveguide elements in an array environment where excitation of asymmetrical higher order modes may create blind spots in the array scan pattern. Another problem is to predict the transmission characteristics of a plane wave incident at any arbitrary angle through an infinitely thin conducting sheet perforated periodically with crossed rectangular shaped apertures. The latter is particularly useful in the design and development of dichroic subreflectors for ground station and spacecraft antenna systems [4].

Modes of crossed rectangular waveguide have been determined by Stalzer *et al.* [5] with the aid of a computer program developed by Konrad and Silvester [6] using the triangular finite element method. In their studies, the transverse fields for each mode can not be obtained in explicit forms for further numerical manipulation. The Ritz–Galerkin method [7] has been successfully applied by Montgomery [8] to obtain the complete eigenvalue solution of dual-ridged waveguides. In this paper an integral-eigenvalue problem is formulated for the crossed rectangular waveguide and solved numerically by applying the Ritz–Galerkin method. The modal fields obtained are in the form of Fourier series which can be conveniently used for phased array analysis and aperture reflection coefficient determination for a waveguide element in an infinite array environment.

Manuscript received June 28, 1976; revised March 22, 1977. This research was supported by the National Aeronautics and Space Administration under contract NAS5-23000.

The author is with Sachs/Freeman Associates, Inc., Hyattsville, MD 20784, for Johns Hopkins University Applied Physics Laboratory, Laurel, MD 20810.

II. Theoretical Formulation

The geometry of the crossed rectangular waveguide is shown in Fig. 1. The plane $x = 0$ is a symmetry plane of the waveguide and the field is calculated for only half of the cross

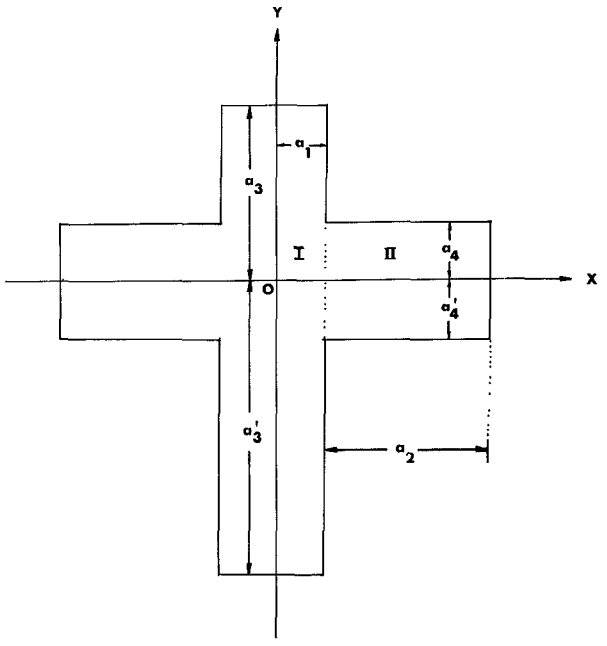

Fig. 1. Geometry of crossed rectangular waveguide.

section ($x > 0$). In general, no symmetry is assumed about the x axis. Hence the eigenvalue problem can be divided into the following four distinct cases:

1) TE-electric mode: TE fields with a metallic wall at $x = 0$;
2) TE-magnetic mode: TE fields with a magnetic wall at $x = 0$;
3) TM-electric mode: TM fields with a metallic wall at $x = 0$;
4) TM-magnetic mode: TM fields with a magnetic wall at $x = 0$.

The text of this paper is based mainly on TE fields with a metallic symmetry plane at $x = 0$. The other three cases are presented in the Appendix.

In a crossed rectangular waveguide with the dimensions shown in Fig. 1, the TE-mode functions $\vec{e}_t(\bar{r}_T)$, where $\bar{r}_T$ is the transverse coordinate vector, are normalized over the entire cross section A

$$\int_A \vec{e}_t^*(\bar{r}_T) \cdot \vec{e}_t(\bar{r}_T)\, dA = 1 \tag{1}$$

and can be derived from the scalar functions $g(\bar{r}_T)$. Note that $g(\bar{r}_T)$ satisfies the wave equation

$$\nabla^2 g(\bar{r}_T) + k_T^2 g(\bar{r}_T) = 0 \tag{2}$$

where k_T is the waveguide eigenvalue. The solutions of this wave equation represent distinct waveguide modes. The cutoff wavelength for mode i, denoted by λ_{ci}, can be calculated from the eigenvalue k_{Ti}, i.e.,

$$\lambda_{ci} = \frac{2\pi}{k_{Ti}}; \qquad i = 1, 2, \cdots. \tag{3}$$

The TE boundary conditions that $\hat{n} \cdot \nabla g = 0$ on a metallic wall, where $\hat{n}$ is the normal to the boundary, yield

$$g_1(\bar{r}_T) = \sum_{n=0}^{\infty} \eta_{1n} \cos(k_{x1n}x) \cdot \cos\left(\frac{n\pi}{a_3 + a_3'}(y - a_3)\right); \qquad 0 \le x \le a_1 \tag{4}$$

and

$$g_2(\bar{r}_T) = \sum_{m=0}^{\infty} \eta_{2m} \cos(k_{x2m}(x - a_2)) \cdot \cos\left(\frac{m\pi}{a_4 + a_4'}(y - a_4)\right); \qquad a_1 \le x \le a_2 \tag{5}$$

for region I and region II, respectively, where

$$k_{x1n} = \begin{cases} \sqrt{k_T^2 - \left(\frac{n\pi}{a_3 + a_3'}\right)^2}; & k_T \ge \frac{n\pi}{a_3 + a_3'} \\ -j\sqrt{\left(\frac{n\pi}{a_3 + a_3'}\right)^2 - k_T^2}; & k_T < \frac{n\pi}{a_3 + a_3'} \end{cases} \tag{6}$$

$$k_{x2m} = \begin{cases} \sqrt{k_T^2 - \left(\frac{m\pi}{a_4 + a_4'}\right)^2}; & k_T \ge \frac{m\pi}{a_4 + a_4'} \\ -j\sqrt{\left(\frac{m\pi}{a_4 + a_4'}\right)^2 - k_T^2}; & k_T < \frac{m\pi}{a_4 + a_4'}. \end{cases} \tag{7}$$

The basis fields are defined as

$$\vec{e}_t(\bar{r}_T) = \nabla g(\bar{r}_T) \times \hat{z}. \tag{8}$$

Hence one can easily derive that for $x > 0$,

$$\vec{e}_1(\bar{r}_T) = -\sum_{n=0}^{\infty} \eta_{1n} \left[\frac{n\pi}{a_3 + a_3'} \cos(k_{x1n}x) \cdot \sin\left(\frac{n\pi}{a_3 + a_3'}(y - a_3)\right)\hat{x} - k_{x1n} \sin(k_{x1n}x) \cdot \cos\left(\frac{n\pi}{a_3 + a_3'}(y - a_3)\right)\hat{y}\right] \tag{9}$$

$$\vec{e}_2(\bar{r}_T) = -\sum_{m=0}^{\infty} \eta_{2m} \left[\frac{m\pi}{a_4 + a_4'} \cos(k_{x2m}(x - a_2)) \cdot \sin\left(\frac{m\pi}{a_4 + a_4'}(y - a_4)\right)\hat{x} - k_{x2m} \sin(k_{x2m}(x - a_2)) \cdot \cos\left(\frac{m\pi}{a_4 + a_4'}(y - a_4)\right)\hat{y}\right] \tag{10}$$

for region I and region II, respectively.

Applying the condition for the continuity of the scalar function at $x = a_1$ and matching the boundary conditions

on the conducting wall result in the following integral equation

$$\sum_{n=0}^{\infty} \frac{\int_{-a_4'}^{a_4} E_g(y') \cos\left(\frac{n\pi}{a_3+a_3'}(y'-a_3)\right) dy'}{k_{x1n}\varepsilon_n(a_3+a_3')} \cdot \cot(k_{x1n}a_1) \cos\left(\frac{n\pi}{a_3+a_3'}(y-a_3)\right)$$

$$= \sum_{m=0}^{\infty} \frac{\int_{-a_4'}^{a_4} E_g(y') \cos\left(\frac{m\pi}{a_4+a_4'}(y'-a_4)\right) dy'}{k_{x2m}\varepsilon_m(a_4+a_4')} \cdot \cot(k_{x2m}(a_1-a_2)) \cos\left(\frac{m\pi}{a_4+a_4'}(y'-a_4)\right) \quad (11)$$

where $E_g(y)$ is the y component of the unknown electric field at $x = a_1$. By application of the Ritz–Galerkin method and expanding $E_g(y)$ in the eigenfunction of region II

$$E_g(y) = \sum_{r=0}^{\infty} C_r \cos\left(\frac{r\pi}{a_4+a_4'}(y-a_4)\right) \quad (12)$$

one obtains[1]

$$\sum_{r=0}^{R} C_r \sum_{n=0}^{N} \frac{\cot(k_{x1n}a_1)}{k_{x1n}\varepsilon_n(a_3+a_3')} P_{nr}P_{nq} = \sum_{r=0}^{R} C_r \frac{\cot(k_{x2q}(a_1-a_2))}{k_{x2q}} \varepsilon_q(a_4+a_4')\delta_{qr}; \quad q = 0, 1, 2, \cdots, R \quad (13)$$

where δ_{qr} is the Kronecker delta, P_{nr} is defined as

$$P_{nr} = \int_{-a_4'}^{a_4} \cos\left(\frac{n\pi}{a_3+a_3'}(y-a_3)\right) \cdot \cos\left(\frac{r\pi}{a_4+a_4'}(y-a_4)\right) dy, \quad (14)$$

$\varepsilon_n = 1$ for $n = 0$ and $\varepsilon_n = \frac{1}{2}$ for $n \neq 0$, and similarly for ε_q. Note that the infinite summations over n and r have been truncated to $(N+1)$ and $(R+1)$ terms, respectively. Equation (13) can also be written as

$$\sum_{r=0}^{R} H_{qr}(k_T)C_r = 0; \qquad q = 0, 1, 2, \cdots, R \quad (15)$$

or conveniently expressed as a matrix equation

$$[H_{qr}]C = 0 \quad (16)$$

with the matrix element $H_{qr}(k_T)$ (the qth row and the rth column) defined as

$$H_{qr}(k_T) = \frac{\cot(k_{x2q}(a_2-a_1))}{k_{x2q}} \varepsilon_q(a_4+a_4')\delta_{qr} + \sum_{n=0}^{N} \frac{\cot(k_{x1n}a_1)}{k_{x1n}\varepsilon_n(a_3+a_3')} P_{nr}P_{nq} \quad (17)$$

[1] The notations and the procedures adopted here are similar to those used in [8] for ridged waveguides.

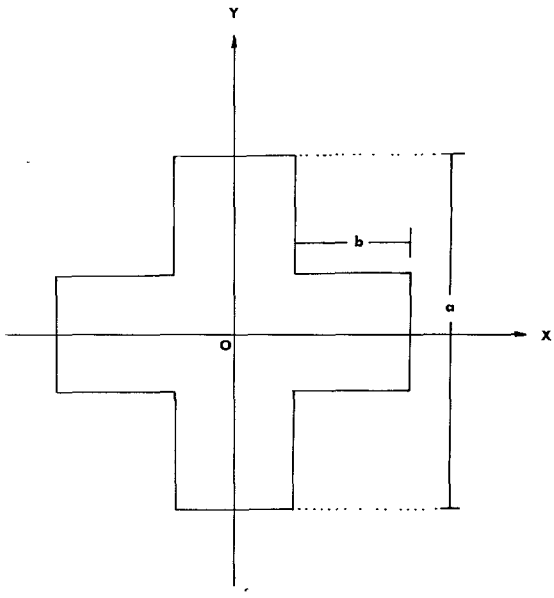

Fig. 2. Configuration of symmetrical crossed rectangular waveguide.

where k_{x1n} and k_{x2q} have been defined in (6) and (7). The determinant of the matrix $[H_{qr}]$ must be zero in order to have nontrivial solutions for this eigenvalue problem. The solutions of the equation

$$\det[H_{qr}] = 0 \quad (18)$$

give the eigenvalues and the corresponding C's are the eigenvectors.

The relationship between C_r, components of eigenvector C, and the coefficients η_{1n}, η_{2m} is given by

$$\eta_{1n} = \frac{\sum_{r=0}^{R} C_r P_{nr}}{k_{x1n} \sin(k_{x1n}a_1)\varepsilon_n(a_3+a_3')} \quad (19)$$

$$\eta_{2m} = \frac{C_m}{k_{x2m} \sin(k_{x2m}(a_1-a_2))}. \quad (20)$$

The modal fields can be subsequently determined.

III. Numerical Solutions and Results

The nonlinear equation (18) for the TE-electric case and the corresponding ones for other three cases are solved by low-order approximation. The convergence of the approximate solution is demonstrated by the variation of the dominant mode TE_{10} (TE-magnetic case) eigenvalue for a symmetrical crossed rectangular waveguide (Fig. 2 with $a = 0.45$ in, $b = 0.1785$ in), as illustrated in Table I. It is shown that all the results agree within one percent but for the lowest orders of approximation. In addition, the convergence of the eigenvalues of higher order mode (TE_{21} mode of TE-electric case as an example) with the same configuration ($a = 0.45$ in, $b = 0.1785$ in) is shown in Table II. Except for the lowest orders of approximation, accuracies of the eigenvalues are within 0.5 percent.

In this work a 10×10 matrix of $[H_{qr}]$ was chosen as a compromise between solution accuracy and the required computation time. The solutions of (18) may be located very

TABLE I
VARIATION OF DOMINANT EIGENVALUE WITH NUMBER OF TERMS IN REGION I AND REGION II

Number of Terms		Dominant Eigenvalue
Region II R+1	Region I N+1	TE_{10} Mode k_T (rad/in)
2	2	7.723287
2	5	7.445809
2	10	7.395242
2	15	7.390151
2	20	7.388413
2	40	7.386748
2	60	7.386440
2	80	7.386332
2	99	7.386287
5	2	7.723658
5	5	7.450720
5	10	7.415417
5	15	7.405985
5	20	7.401436
5	40	7.396310
5	60	7.395450
5	80	7.394883
5	99	7.394693
10	2	7.723697
10	5	7.451198
10	10	7.416476
10	15	7.407659
10	20	7.403908
10	40	7.398945
10	60	7.397131
10	80	7.396788
10	99	7.396656
15	2	7.723703
15	5	7.451277
15	10	7.416646
15	15	7.407914
15	20	7.404246
15	40	7.399703
15	60	7.398357
15	80	7.397486
15	99	7.397271

TABLE II
VARIATION OF TE_{21} MODE EIGENVALUE WITH NUMBER OF TERMS IN REGION I AND REGION II

Number of Terms		TE_{21} Mode Eigenvalue
Region II R+1	Region I N+1	k_T (rad/in)
2	5	21.925655
2	10	21.884446
2	15	21.876697
2	20	21.874692
2	40	21.872954
2	60	21.872647
2	80	21.872539
2	99	21.872488
5	5	21.940361
5	10	21.912136
5	15	21.902429
5	20	21.897010
5	40	21.888971
5	60	21.888275
5	80	21.888042
5	99	21.887934
10	5	21.942444
10	10	21.915077
10	15	21.906243
10	20	21.901946
10	40	21.895400
10	60	21.892428
10	80	21.891952
10	99	21.891753
15	5	21.942830
15	10	21.915610
15	15	21.906905
15	20	21.902733
15	40	21.896791
15	60	21.894764
15	80	21.893237
15	99	21.892882

close to singularities and care must be taken in the root-finding process. A program was written for the IBM 360/95 computer. The values of det $[H_{qr}]$ were determined when k_T was scanned over the region of interest. The program automatically decreases the incremental size of k_T when a change in sign of det $[H_{qr}]$ takes place. It can resolve the roots with little separation and those located in the neighborhood of singularities. The corresponding eigenvector components C_r for a particular eigenvalue k_T can be obtained from (15). All the C_r's with $r \neq 0$ are evaluated in terms of C_0. Since the basis field $\vec{e}_t(\bar{r}_T)$ consists of two parts

$$\vec{e}_t(r_T) = \begin{cases} \vec{e}_t^{+}(\bar{r}_T); & x > 0 \\ \vec{e}_t^{-}(\bar{r}_T); & x < 0 \end{cases} \tag{21}$$

where

$$\vec{e}_t^{+}(r_T) = \begin{cases} \vec{e}_1(\bar{r}_T); & \text{region I} \\ \vec{e}_2(\bar{r}_T); & \text{region II} \end{cases}$$

and $\vec{e}_t^{-}(\bar{r}_T)$ can be obtained from $\vec{e}_t^{+}(\bar{r}_T)$ by appropriate symmetry conditions, subsequent normalization of $e_t(\bar{r}_T)$ [see equation (1)] yields the value of C_0.

The normalized modal cutoff frequencies (a/λ_c) of a symmetrical crossed rectangular waveguide are determined and shown in Figs. 3–6 as a function of the ratio b/a for all four distinct modes. For the case of $b/a = 0$, the cutoff frequencies indeed coincide with those of the square waveguide of dimension a. As a consequence, the modal designations are referred to those in square waveguide with

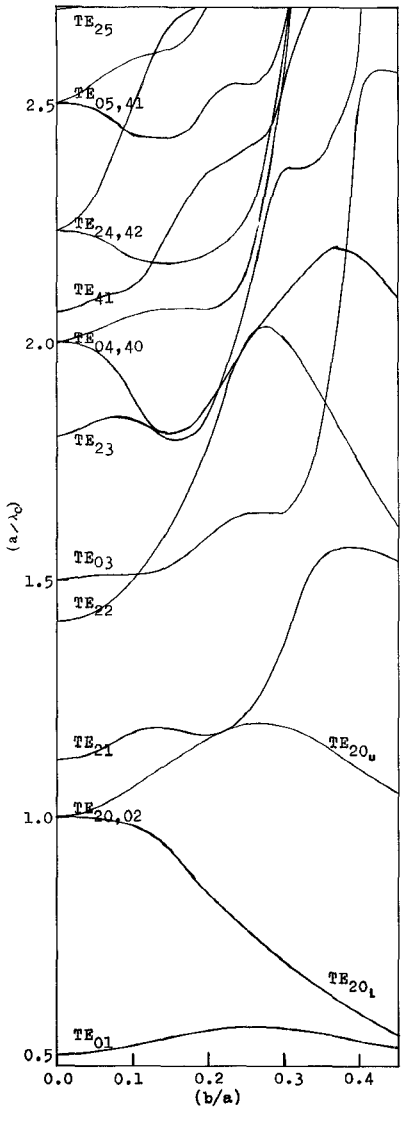

Fig. 3. Normalized cutoff frequencies as a function of b/a for TE-electric modes.

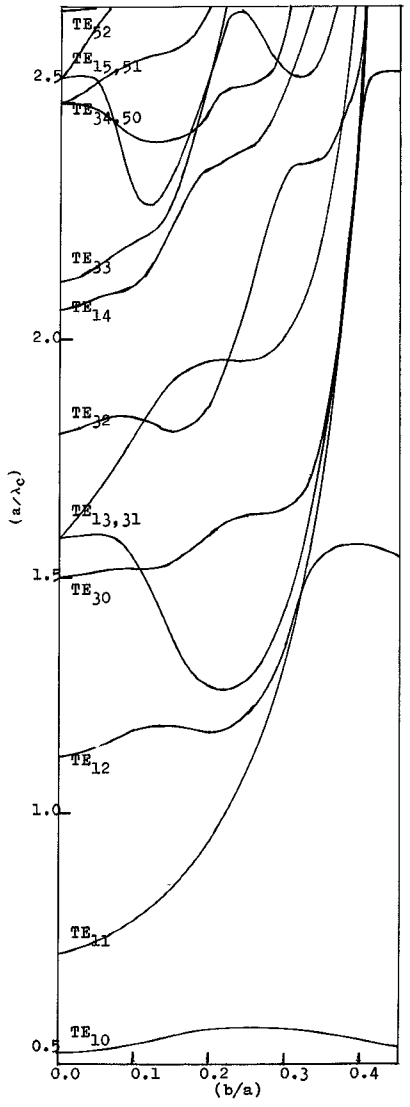

Fig. 4. Normalized cutoff frequencies as a function of b/a for TE-magnetic modes.

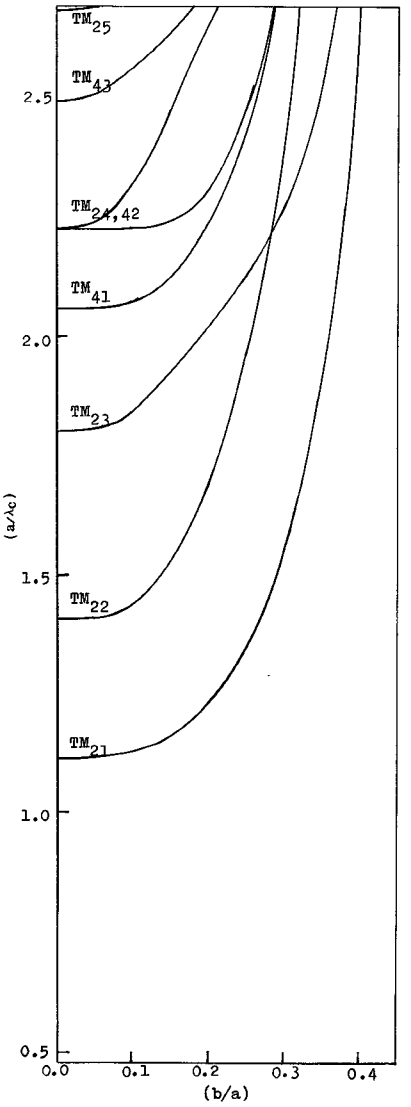

Fig. 5. Normalized cutoff frequencies as a function of b/a for TM-electric modes.

the corresponding boundary conditions. Note for several lower order modes, ridge loading on the corners of a square waveguide raises the cutoff frequencies of the TE_{11},TM_{11} modes (Fig. 4, Fig. 6), and splits the TE_{20},TE_{02} modes into TE_{20_L} and TE_{20_U} modes, lifting the orthogonal degeneracy (Fig. 3). However, the degeneracy of the TE_{01} and TE_{10} modes is retained, as can be seen from Figs. 3 and 4, in spite of ridge loading. The cutoff frequencies calculated for TE_{10}, TE_{11}, and TM_{11} modes agree with the experimental results [5] within one percent except in a couple of points. For higher order modes TE_{ij} and TE_{ji} (or TM_{ij} and TM_{ji}) modes (i = even, j = odd or vice versa) remain degenerate, whereas the degeneracies of TE_{ij} and TE_{ji} (or TM_{ij} and TM_{ji}) modes (i = even, j = even, $i \neq j$; or i = odd, j = odd, $i \neq j$) in a square waveguide are destroyed by ridge loading.

The bandwidth percentage of a waveguide is defined as

$$BW = \frac{\lambda_{c-} - \lambda_{c+}}{\lambda_{c-} + \lambda_{c+}} \times 200 \text{ percent} \qquad (22)$$

where λ_{c-} is the cutoff wavelength of the fundamental mode, and λ_{c+} is the cutoff wavelength of the first higher order mode. The bandwidth characteristics for symmetrical crossed rectangular waveguides have been calculated and plotted in Fig. 7. The maximum bandwidth (about 38 percent) incurs when $b/a = 0.225$. To the left of the peak as shown in Fig. 7, the bandwidth is determined by the TE_{10} and TM_{11} modes, whereas to the right by the TE_{10} and TE_{20} modes. This feature of a 38-percent maximum bandwidth over the 34 percent for a square waveguide makes the symmetrical crossed rectangular waveguide compatible with the quadruple-ridged circular waveguide [2]. However, if asymmetrical excitation is applied, the maximum bandwidth of 66 percent can be achieved when $b/a = 0.325$ where TM_{11} mode is the deciding factor.

IV. Conclusion

Theoretical formulas for finding cutoff frequencies and modal field expressions are obtained for crossed rectangular

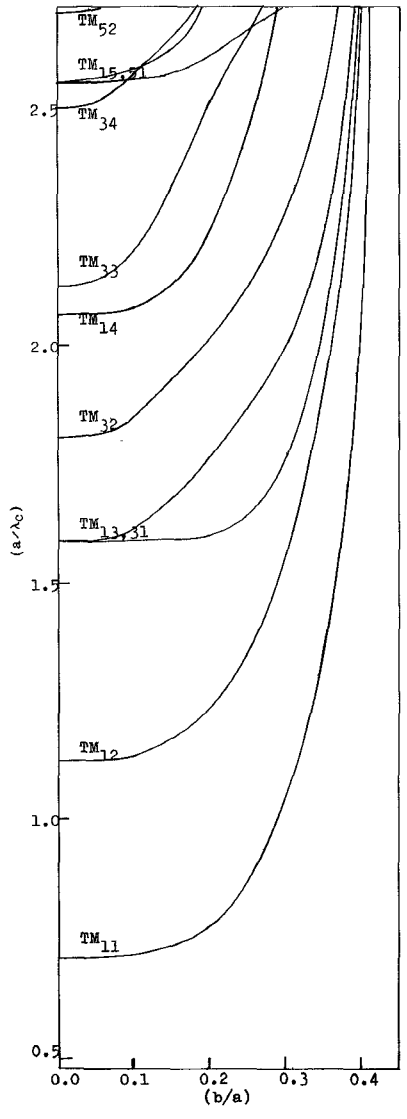

Fig. 6. Normalized cutoff frequencies as a function of b/a for TM-magnetic modes.

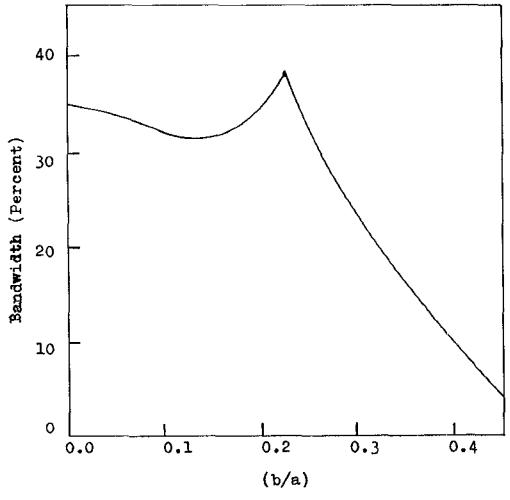

Fig. 7. Bandwidth characteristic curve for symmetrical crossed rectangular waveguide.

waveguide by application of the Ritz–Galerkin method. A specific example of a symmetrical rectangular waveguide is chosen. Cutoff frequencies are calculated numerically and verified by available experimental data. The bandwidth can be increased to a maximum of 38 percent when waveguide dimensions are properly selected. The numerical results obtained here agree with those by the method of partial regions [9]. It is believed that the modal field equations formulated here can be used in a modal matching technique [10], [11] to predict transmission characteristics of a plane wave through a thin conducting sheet perforated periodically with crossed rectangular shaped apertures.

Appendix

A. TE-Magnetic Mode

The electric fields in regions I and II are given by

$$\vec{e}_1(\bar{r}_T) = -\sum_{n=0}^{L} \eta_{1n} \left[\frac{n\pi}{a_3 + a_3'} \sin(k_{x1n}x) \cdot \sin\left(\frac{n\pi}{a_3 + a_3'}(y - a_3)\right)\hat{x} + k_{x1n}\cos(k_{x1n}x) \cdot \cos\left(\frac{n\pi}{a_3 + a_3'}(y - a_3)\right)\hat{y} \right] \tag{23}$$

$$\vec{e}_2(\bar{r}_T) = -\sum_{m=0}^{M} \eta_{2m} \left[\frac{m\pi}{a_4 + a_4'} \cos(k_{x2m}(x - a_2)) \cdot \sin\left(\frac{m\pi}{a_4 + a_4'}(y - a_4)\right)\hat{x} - k_{x2m}\sin(k_{x2m}(x - a_2)) \cdot \cos\left(\frac{m\pi}{a_4 + a_4'}(y - a_4)\right)\hat{y} \right]. \tag{24}$$

Making the expansion

$$E_g(y) = \sum_{r=0}^{R} C_r \cos\left(\frac{r\pi}{a_4 + a_4'}(y - a_4)\right) \tag{25}$$

one finds that the matrix elements are given by

$$H_{qr}(k_T) = -\frac{\cot(k_{x2q}(a_2 - a_1))}{k_{x2q}} \varepsilon_q(a_4 + a_4')\delta_{qr} + \sum_{n=0}^{L} P_{nr}P_{nq} \frac{\tan(k_{x1n}a_1)}{k_{x1n}\varepsilon_n(a_3 + a_3')}. \tag{26}$$

The relations between field coefficients and eigenvector components are

$$\eta_{1n} = \frac{-\sum_{r=0}^{R} C_r P_{nr}}{k_{x1n}\cos(k_{x1n}a_1)\varepsilon_n(a_3 + a_3')} \tag{27}$$

$$\eta_{2m} = \frac{-C_m}{k_{x2m}\sin(k_{x2m}(a_2 - a_1))}. \tag{28}$$

B. TM-Electric Mode

The transverse electric fields in regions I and II are given by

$$\vec{e}_1(\bar{r}_T) = \sum_{n=1}^{L} \xi_{1n} \left[k_{x1n} \cos (k_{x1n}x) \cdot \sin\left(\frac{n\pi}{a_3 + a_3'}(y - a_3)\right)\hat{x} + \frac{n\pi}{a_3 + a_3'} \sin (k_{x1n}x) \cdot \cos\left(\frac{n\pi}{a_3 + a_3'}(y - a_3)\right)\hat{y} \right] \quad (29)$$

$$\vec{e}_2(\bar{r}_T) = \sum_{m=1}^{M} \xi_{2m} \left[k_{x2m} \cos (k_{x2m}(x - a_2)) \cdot \sin\left(\frac{m\pi}{a_4 + a_4'}(y - a_4)\right)\hat{x} + \frac{m\pi}{a_4 + a_4'} \sin (k_{x2m}(x - a_2)) \cdot \cos\left(\frac{m\pi}{a_4 + a_4'}(y - a_4)\right)\hat{y} \right]. \quad (30)$$

The z components of the electric field are given by

$$\vec{e}_{1z}(\bar{r}_T) = \sum_{n=1}^{L} \xi_{1n} \sin (k_{x1n}x) \cdot \sin\left(\frac{n\pi}{a_3 + a_3'}(y - a_3)\right)\hat{z} \quad (31)$$

$$e_{2z}(\bar{r}_T) = \sum_{m=1}^{M} \xi_{2m} \sin (k_{x2m}(x - a_2)) \cdot \sin\left(\frac{m\pi}{a_4 + a_4'}(y - a_4)\right)\hat{z}. \quad (32)$$

Making the expansion

$$E_g(y) = \sum_{r=1}^{L} C_r \sin\left(\frac{r\pi}{a_4 + a_4'}(y - a_4)\right) \quad (33)$$

one finds that the matrix elements are given by

$$H_{qr}(k_T) = k_{x2q} \cot (k_{x2q}(a_2 - a_1))\tfrac{1}{2}(a_4 + a_4')\delta_{qr} + 2 \sum_{n=1}^{L} P'_{nr}P'_{nq}k_{x1n} \cot (k_{x1n}a_1)/(a_3 + a_3') \quad (34)$$

where

$$P'_{nr} = \int_{-a_4'}^{a_4} \sin\left(\frac{n\pi}{a_3 + a_3'}(y - a_3)\right) \cdot \sin\left(\frac{r\pi}{a_4 + a_4'}(y - a_4)\right) dy. \quad (35)$$

The relations between field coefficients and eigenvector components are

$$\xi_{1n} = \frac{\sum_{r=1}^{L} C_r P'_{nr}}{\sin (k_{x1n}a_1)\tfrac{1}{2}(a_3 + a_3')} \quad (36)$$

$$\xi_{2m} = \frac{-C_m}{\sin (k_{x2m}(a_2 - a_1))}. \quad (37)$$

C. TM-Magnetic Mode

The transverse electric fields in regions I and II are given by

$$\vec{e}_1(\bar{r}_T) = -\sum_{n=1}^{L} \xi_{1n} \left[k_{x1n} \sin (k_{x1n}x) \cdot \sin\left(\frac{n\pi}{a_3 + a_3'}(y - a_3)\right)\hat{x} - \frac{n\pi}{a_3 + a_3'} \cos (k_{x1n}x) \cdot \cos\left(\frac{n\pi}{a_3 + a_3'}(y - a_3)\right)\hat{y} \right] \quad (38)$$

$$\vec{e}_2(\bar{r}_T) = \sum_{m=1}^{M} \xi_{2m} \left[k_{x2m} \cos (k_{x2m}(x - a_2)) \cdot \sin\left(\frac{m\pi}{a_4 + a_4'}(y - a_4)\right)\hat{x} + \frac{m\pi}{a_4 + a_4'} \sin (k_{x2m}(x - a_2)) \cdot \cos\left(\frac{m\pi}{a_4 + a_4'}(y - a_4)\right)\hat{y} \right]. \quad (39)$$

The z components of the electric field are given by

$$\vec{e}_{1z}(\bar{r}_T) = \sum_{n=1}^{L} \xi_{1n} \cos (k_{x1n}x) \cdot \sin\left(\frac{n\pi}{a_3 + a_3'}(y - a_3)\right)\hat{z} \quad (40)$$

$$\vec{e}_{2z}(\bar{r}_T) = \sum_{m=1}^{M} \xi_{2m} \sin (k_{x2m}(x - a_2)) \cdot \sin\left(\frac{m\pi}{a_4 + a_4'}(y - a_4)\right)\hat{z}. \quad (41)$$

Making the expansion

$$E_g(y) = \sum_{r=1}^{L} C_r \sin\left(\frac{r\pi}{a_4 + a_4'}(y - a_4)\right) \quad (42)$$

one finds that the matrix elements are given by

$$H_{qr}(k_T) = k_{x2q} \cot (k_{x2q}(a_2 - a_1))\tfrac{1}{2}(a_4 + a_4')\delta_{qr} - 2 \sum_{n=1}^{L} P'_{nr}P'_{nq}k_{x1n} \tan (k_{x1n}a_1)/(a_3 + a_3'). \quad (43)$$

The relations between field coefficients and eigenvector components are

$$\xi_{1n} = \frac{\sum_{r=1}^{L} C_r P'_{nr}}{\cos\left(k_{x1n} a_1\right) \frac{1}{2}(a_3 + a'_3)} \tag{44}$$

$$\xi_{2m} = \frac{-C_m}{\sin\left(k_{x2m}(a_2 - a_1)\right)}. \tag{45}$$

References

[1] G. N. Tsandoulas and G. H. Knittel, "The analysis and design of dual-polarization square-waveguide phased arrays," *IEEE Trans. Antennas Propagat.*, vol. AP-21, pp. 796–808, Nov. 1973.

[2] M. H. Chen, G. N. Tsandoulas, and F. G. Willwerth, "Modal characteristics of quadruple-ridged circular and square waveguides," *IEEE Trans. Microwave Theory Tech.*, vol. MTT-22, pp. 801–804, Aug. 1974.

[3] P. Silvester, "A general high-order finite-element waveguide analysis program," *IEEE Trans. Microwave Theory Tech.*, vol. MTT-17, pp. 204–210, Apr. 1969.

[4] T. E. Wise, "Final report, dichroic surface analysis: *S*-, *X*-, and *K*-band," Bendix Field Engineering Corporation Rep., Mar. 1975 (unpublished).

[5] H. J. Stalzer, Jr., M. D. Greenman, and F. G. Willwerth, "Modes of crossed rectangular waveguide," *IEEE Trans. Antennas Propagat.*, vol. AP-24, pp. 220–223, Mar. 1976.

[6] A. Konrad and P. Silvester, "Scalar finite-element program package for two-dimensional field problems," *IEEE Trans. Microwave Theory Tech.*, vol. MTT-19, pp. 952–954, Dec. 1971.

[7] R. F. Harrington, *Field Computation by Moment Method.* New York: Macmillan, 1968.

[8] J. P. Montgomery, "On the complete eigenvalue solution of ridged waveguide," *IEEE Trans. Microwave Theory Tech.*, vol. MTT-19, pp. 547–555, June 1971.

[9] Q. C. Tham, "Modes and cutoff frequencies of crossed rectangular waveguides," Bendix Field Engineering Corporation Rep., May 1976 (to be published).

[10] C. C. Chen, "Transmission through a conducting screen perforated periodically with apertures," *IEEE Trans. Microwave Theory Tech.*, vol. MTT-18, pp. 627–632, Sept. 1970.

[11] ——, "Diffraction of electromagnetic waves by a conducting screen perforated periodically with circular apertures," *IEEE Trans. Microwave Theory Tech.*, vol. MTT-19, pp. 475–481, May 1971.

Iterative Solutions of Waveguide Discontinuity Problems

MAGDY F. ISKANDER, MEMBER, IEEE, AND M. A. K. HAMID, SENIOR MEMBER, IEEE

Abstract—**The method of overlapping regions, together with Schwarz's technique, is applied to waveguide discontinuity problems to illustrate its potential and basic advantages and disadvantages over other methods. The method reasonably corrects an arbitrary initial assumption of field distribution in the plane of discontinuity to the final value in a small number of iterations. The advantages are illustrated for a waveguide bend and dumbbell shaped waveguide as examples of transverse and longitudinal discontinuities, respectively. Numerical results for the case where only the electric field is parallel to the sharp edge discontinuity are presented and compared with available data, while extension to the case where only the magnetic field is parallel to the edge is discussed.**

I. Introduction

SHARP waveguide discontinuities are extensively used in numerous microwave power and communication circuits, and their effects have been under investigation in the last few decades. Generally, these discontinuities are characterized as either transverse or longitudinal, depending on whether the discontinuity lies in a plane transverse or parallel to the direction of propagation, respectively, or both. Waveguide junctions and bends are typical examples of transverse discontinuities, while waveguide complex cross sections belong to the class of longitudinal discontinuities.

Earlier attempts to characterize such discontinuities include rigorous, quasi-rigorous, numerical, and experimental techniques [1]–[4]. The results normally permit computation of scattering matrix parameters, which may be used to evaluate the parameters of an equivalent circuit, cutoff wave numbers, and mode coefficients leading to propagation coefficients and field configurations.

While no method can be expected to deal with the most general case of mixed types of discontinuities and arbitrary waveguide boundaries, the choice of one method over others for the most common discontinuities depends on the shape as well as the electrical and physical dimensions of the waveguide. Thus due to its asymptotic nature, the geometrical theory of diffraction, in which the discontinuity is viewed as multiple body interaction, becomes more appropriate as the smallest linear dimension exceeds one wavelength [5]. However, when the distances between edges and corners are

Manuscript received August 16, 1976; revised February 23, 1977. This research was supported in part by the National Research Council of Canada through Grant 43326.

M. F. Iskander was with the Antenna Laboratory, Department of Electrical Engineering, University of Manitoba, Winnipeg, Manitoba, R3T 2N2, Canada. He is now with the Department of Electrical Engineering and the Department of Bioengineering, University of Utah, Salt Lake City, UT 84112.

M. A. K. Hamid is with the Antenna Laboratory, Department of Electrical Engineering, University of Manitoba, Winnipeg, Manitoba, R3T 2N2, Canada.